Experimental investigations of bubble chains in a liquid metal under the influence of a horizontal magnetic field

Keplinger, O.; Shevchenko, N.; Eckert, S.;

Originally published:

December 2019

International Journal of Multiphase Flow 121(2019), 103111

DOI: https://doi.org/10.1016/j.ijmultiphaseflow.2019.103111

Perma-Link to Publication Repository of HZDR:

https://www.hzdr.de/publications/Publ-29223

Experimental investigations of bubble chains in a liquid metal under the influence of a horizontal magnetic field

Olga Keplinger, Natalia Shevchenko, Sven Eckert.

Abstract

We present an experimental study on bubble chains ascending in the eutectic GaInSn alloy under the influence of a horizontal magnetic field. Argon gas bubbles are injected through a single nozzle positioned in the middle at the bottom of a flat Plexiglas vessel. Bubble size distribution, shape deformation, velocities, etc. are obtained by post-processing of X-ray radiographs measured with a high-speed video-camera for a wide range of Argon gas flow rates. In the case without a magnetic field, the typical zigzag movement of the rising bubbles is observed. This movement and the integrity of the bubble chain are significantly disturbed with increasing gas flow by the turbulent flow in the liquid metal. The main effect of the magnetic field consists in a stabilization of the bubble trajectories. The application of a magnetic field at moderate field strength dampens the turbulent fluctuations in the bubble wake and stabilizes the zigzag movement. The application of a sufficiently strong magnetic field suppresses the zig-zag motion of the bubbles and forces them to follow a straight path. The rising velocity is gradually reduced with increasing magnetic field strength. The motion of the individual bubbles within the chain becomes highly correlated. Ellipsoidal bubbles tend to align their major axes along the magnetic field lines.

Key words: Liquid metal; Two-phase flow; Bubble chain; Horizontal magnetic field; X-ray radiography.

Introduction

Liquid metal two-phase flows are an essential feature in many metallurgical processes. For instance, gas bubbles are injected in ladles for mixing and homogenization of the melt as well as for removing undesired inclusions by transporting them towards the slag layer at the free surface. During continuous casting Argon gas is added to the steel flow in the submerged entry nozzle to avoid clogging. The optimization of the processes in terms of efficiency and product quality requires a deep understanding of the fluid dynamics and the availability of flexible and powerful tools for flow control. Therefore, key properties of the two-phase flow (flow regime, gas distribution, void fraction, bubble properties, etc.) are a matter of particular interest.

Different types of magnetic fields are employed in practice to improve, to some extent, the product quality and the efficiency of metallurgical and casting processes by controlling the fluid flow. The fluid dynamics of dispersed, compressible flows in general, and the impact of external magnetic fields on both the turbulent liquid metal flow and the behavior of the gas phase in particular, are known to be extremely complex. The number of numerical and experimental papers dealing with liquid metal two-phase flows is constantly growing, however, only a few studies focus on bubble rise in the presence of a magnetic field.

A couple of previous studies consider the behavior of single bubbles in a DC magnetic field. Both horizontally and vertically applied magnetic fields cause a straightening of the bubble path (Fröhlich et al., 2013; Jin et al., 2016; Mori et al., 1977; Richter et al., 2018; Schwarz and Fröhlich, 2014; Zhang et al., 2005). The zig-zag trajectory of middle-sized bubbles (for instance 5 mm argon bubbles in GaInSn) triggered by the undulating wake structure undergoes significant modifications in a vertical magnetic field: the bubble wake is substantially stretched in the vertical direction and the smallest structures of the vorticity are considerably damped (Fröhlich et al., 2013; Zhang et al., 2005, 2016). Numerical simulations by (Schwarz and Fröhlich, 2014; Zhang and Ni, 2014) show that without a magnetic field the vortex threads in the bubble wake wrap around each other, while vortex filaments become aligned parallel to the field with increasing magnetic field strength. Moreover, Zhang and Ni (2014) predicted the occurrence of the so-called secondary bubble path instabilities at moderate vertical magnetic fields corresponding to magnetic interaction parameters N (definition will be given below) in the range of 1.5 - 2.4. This instability vanishes for higher magnetic field intensities (N = 65) and was not predicted in horizontal magnetic fields (Jin et al., 2016). An experimental verification of such path instability in vertical magnetic fields is still pending. Richter et al. (2018) investigated instabilities of the bubble trajectories occurring both without magnetic field and under the influence of a horizontal magnetic field. They reported initial path instabilities in the zig-zag trajectory. Here, extreme changes in the orientation of an ellipsoidal bubble have been observed, it is even possible that the bubble performs movements that are reminiscent of a "somersault". This phenomenon vanishes beyond a critical value of the applied horizontal magnetic field. In the situation of large horizontal magnetic fields the hairpin wake structures behind the bubble almost disappear (Jin et al., 2016).

The influence of both the vertical and the horizontal magnetic field on the bubble velocity is dominated by two effects. On one hand, the magnetic field stabilizes the bubble path (damping of the zig-zag motion) leading to an acceleration of the bubble in vertical direction. On the other hand, the bubble velocity is decreased by the braking effect on the fluid flow around the bubble. The resulting behavior depends essentially on the bubble size. Experiments in GaInSn in a vertical field revealed an increase of the drag coefficient for smaller bubbles ($d_B \leq 4.6$ mm) with increasing magnetic field while larger bubbles ($d_B \geq 5.4$ mm) experience a reduction of the drag coefficient (Zhang et al., 2005). For small bubbles ($d_B = 2$ mm) rising in mercury under the impact of a horizontal field the average bubble rise velocity shows a maximum and then decreases with increasing field strength, whereas a growing magnetic field causes a continuous deceleration of larger bubbles ($d_B = 6$ mm) (Mori et al., 1977). This behavior was reproduced by respective numerical simulations (Jin et al., 2016; Schwarz and Fröhlich, 2014; Wang et al., 2017). The drop of the terminal velocity at high magnetic fields yields to a significant restructuring of the global flow pattern and reduces the intensity of the large-scale circulation in the container (Fröhlich et al., 2013). Moreover, the shape of the velocity oscillations appear more regular and the amplitude decreases with increasing magnetic field (Schwarz and Fröhlich, 2014; Zhang et al., 2005). The oscillation amplitudes of the bubble tilting angle (Schwarz and Fröhlich, 2014) and of the bubble shape decrease with increasing magnetic field, too (Jin et al., 2016).

All studies discussed above are concerned with the behavior of single bubbles in magnetic fields. However, industrial applications apply gas injection at higher gas flow rates leading to the formation of bubble chains and plumes. The situation here is more complex because the flow is highly turbulent and the bubble rising dynamics becomes affected by bubble-wake and bubble-bubble interactions. Investigations in bubble plumes show that the presence of DC magnetic fields has a strong effect on the turbulent velocity fluctuations in the liquid. However, the direction of the magnetic field with respect to the ascent direction of the bubbles plays an essential role. Whereas a global damping of the turbulent flow was

observed in case of a vertical magnetic field, the application of a horizontal magnetic field can induce a restructuring of the flow field accompanied by the appearance of pronounced velocity oscillations arising from non-steady vortical structures (Zhang et al., 2007a, 2007b). Such a peculiar behavior could be relevant for industrial processes as the application of electromagnetic brakes during the continuous casting of steel. The magnetic field also changes the gas distribution in the cross section of the fluid vessel. Eckert et al. (2000a) have shown that the gas distribution is almost isotropic in a vertical magnetic field, while an anisotropic gas distribution is observed in case of a horizontal magnetic field, namely the gas dispersion in the direction parallel to the magnetic field is effectively suppressed. For high values of the magnetic field the gas distribution is considerably restricted to a narrow area around the position of the gas injection for both directions of the magnetic field.

So far, there are only very few experimental studies on the dynamics of bubble motion in liquid metals. The main reason is the limitation with respect to the measuring techniques for characterizing two-phase flows in nontransparent liquids. Essential bubble parameters as for example the bubble size, the shape and its deformation were only demonstrated numerically mainly because the opacity of the metals does not allow the utilization of powerful optical methods. Local conductivity probes (Davenport et al., 1967; Eckert et al., 2000a, 2000b; Iguchi et al., 1997; Manera et al., 2009; Oryall and Brimacombe, 1976; Xie et al., 1992; Xie and Oeters, 1994), ultrasound techniques (Richter et al., 2018; Timmel et al., 2010; Wang et al., 2017; Zhang et al., 2005) or inductive methods (Gundrum et al., 2016; Lyu and Karcher, 2016) can be applied to detect gas bubbles in liquid metals. However, all these methods are subject to certain restrictions. For example, conductivity probes are intrusive and provide only local information. Ultrasonic methods encounter problems when the number of bubbles in the measuring volume increases with increasing gas content. Multiple echoes at the bubble interfaces can create signal artifacts causing serious difficulties in data processing. Inductive methods provide a contactless method for bubble detection in liquid metal flows, but, the reconstruction of the bubble shape is still challenging and the interpretation of the signals becomes exceedingly difficult in case of multiple bubble-bubble interaction. X-ray radiography based on the absorption contrast between the liquid and gas phase has proven to be an efficient method for multiphase flows (Heindel, 2011; Kastengren and Powell, 2014; Mudde, 2010; Mudde et al., 2008) and especially for bubble detection in liquid metals (Davis et al., 1978; Fröhlich et al., 2013; Iguchi et al., 1995; Keplinger et al., 2018; Richter et al., 2018; Shevchenko et al., 2013; Timmel et al., 2015; Vogt et al., 2015; Wang et al., 1999). The main limitation of this technique is the high X-ray absorption coefficient of the liquid metals which allows measurements with sufficient image contrast only for a limited thickness of the liquid volume. The accuracy of the X-ray radiography technique for determining bubble parameters is discussed in detail in (Keplinger et al., 2017). Another irradiation method is the neutron radiography (Baake et al., 2017; Mishima et al., 1999; Saito et al., 2005; Sarma et al., 2015) which allows the investigation of thicker measuring volumes but at the expense of image contrast.

In the present paper we focus on bubble chains rising in a liquid metal in a horizontal magnetic field. The dynamics of the bubbly flow was visualized by means of X-ray radiography using high-speed imaging. The objective of our study is to investigate the effect of the magnetic field on the behavior of single bubbles in the chain and the interaction between adjacent bubbles. The bubble-bubble interaction is mainly governed by the exchange of momentum in the bubble wake. Some previous studies (Jin et al., 2016; Zhang et al., 2016) provided clear indications that the bubble wake is significantly affected by the magnetic field, however, a direct visualization of the process is not available yet. Hereinafter, we present a statistical analysis concerning the bubble rising velocity, the bubble orientation and the deformation of the bubble shape for different magnetic field intensities and gas flow rates.

Experimental setup

Bubble visualization experiments were carried out at the X-ray laboratory at HZDR. The model fluid is the ternary alloy GaInSn, which eutectic composition is liquid at room temperature and whose material properties are very similar to those of liquid steel (Plevachuk et al., 2014). The scheme of the experimental setup is shown in Figure 1a. The fluid vessel was made of acrylic glass and has the form of a cuboid with a rectangular cross-section of 86×12 mm^2. It was filled with GaInSn up to a height of 129 mm resulting in a total aspect ratio of 1.5. This aspect ratio guaranties bubble chain oscillation and therefore intensive melt mixing (Liu et al., 2019, 2018). The inert Argon gas was injected through a single long bevel-shaped stainless steel orifice with an inner diameter of 0.75 mm (from Sterican®) positioned in the middle of the cross-section just above the bottom of the vessel. Such a nozzle shape was preferred over a flat nozzle in order to prevent the bubble zig-zag motion between the walls in the direction of the X-ray beam. The gas flow rate was regulated in the range from 150 to 1200 cm^3/min by a gas flow control system from MKS Instruments. The experiments were conducted at room temperature and normal atmospheric pressure.

The vessel was positioned in the middle of the magnetic system (custom-made design by Schueler Magnetic LTD) composed of two opposite permanent magnets. This arrangement produces a non-uniform horizontal magnetic field pointing perpendicular to the direction of the X-ray beam. The distance between the magnets can be adjusted in the range from 100 to 150 mm (see Figure 1b) which allows achieving magnetic fields of different strengths. The mapping of the magnetic field for the two configurations used in this manuscript is shown in Figure 1 c and d. The magnetic field strength (B) reaches value of ~156 mT and ~262 mT in the center of the magnetic system for a pole shoe gap of 150 mm and 100 mm, respectively. The field strength increases towards the magnets and decreases with growing distance from the center along the vertical direction. There is no considerable magnetic field gradient in the fluid vessel in the direction of the X-ray beam, since the extent in this direction is significant less than the dimensions of the magnetic pole pieces.

The behavior of the gas bubbles rising in the magnetic field can be characterized by non-dimensional parameters as the Reynolds number $Re = \frac{\rho d_B u_T}{\gamma}$, the magnetic interaction parameter $N = \frac{\sigma B^2 d_B}{\rho u_T}$ and the Hartmann number $Ha = B d_B \sqrt{\sigma/\nu}$, where σ is the electrical conductivity, ρ is the liquid metal density, ν is the liquid metal viscosity, d_B is the bubble diameter and u_T is the bubble terminal velocity.

A continuous divergent polychromatic X-ray beam was generated using a customary X-ray tube (ISOVOLT 450KV/25-55, GE Sensing & Inspecting Technologies GmbH) at a voltage of 320 kV and a current of 14 mA. The X-ray beam penetrates the liquid metal along the narrow extension of the fluid container as shown in Figure 1a. The non-absorbed part of the beam impinges on a scintillation screen (i.e. scintillator for medical application) that is attached to the outer wall of the vessel. The corresponding intensity I can be estimated by the Beer-Lambert law:

$$I = I_0 e^{-\mu D}, \qquad (1)$$

where I_0 is the primary beam intensity, μ is the X-ray attenuation coefficient and D is the thickness of the liquid metal. The X-ray intensity is then converted into visible light in the scintillator that is further deflected by a mirror through a lens system (custom-made design by Thalheim-Spezial-Optik) onto a sCMOS sensor plane of the high-speed video camera (pco.edge 5.5 from PCO). The camera field of view

(FOV) was ~80×140 mm^2. In the selected experiments the images were captured with 150 frames per second. An exposure time of 3 milliseconds was chosen resulting in a suitable signal-to-noise ratio without causing significant blurring of the quickly ascending bubbles. Additionally, a slit and two collimators are installed to cut the X-ray beam leading to an effective reduction of undesirable X-ray scattering by the room environment which otherwise contributes to the measurement signal.

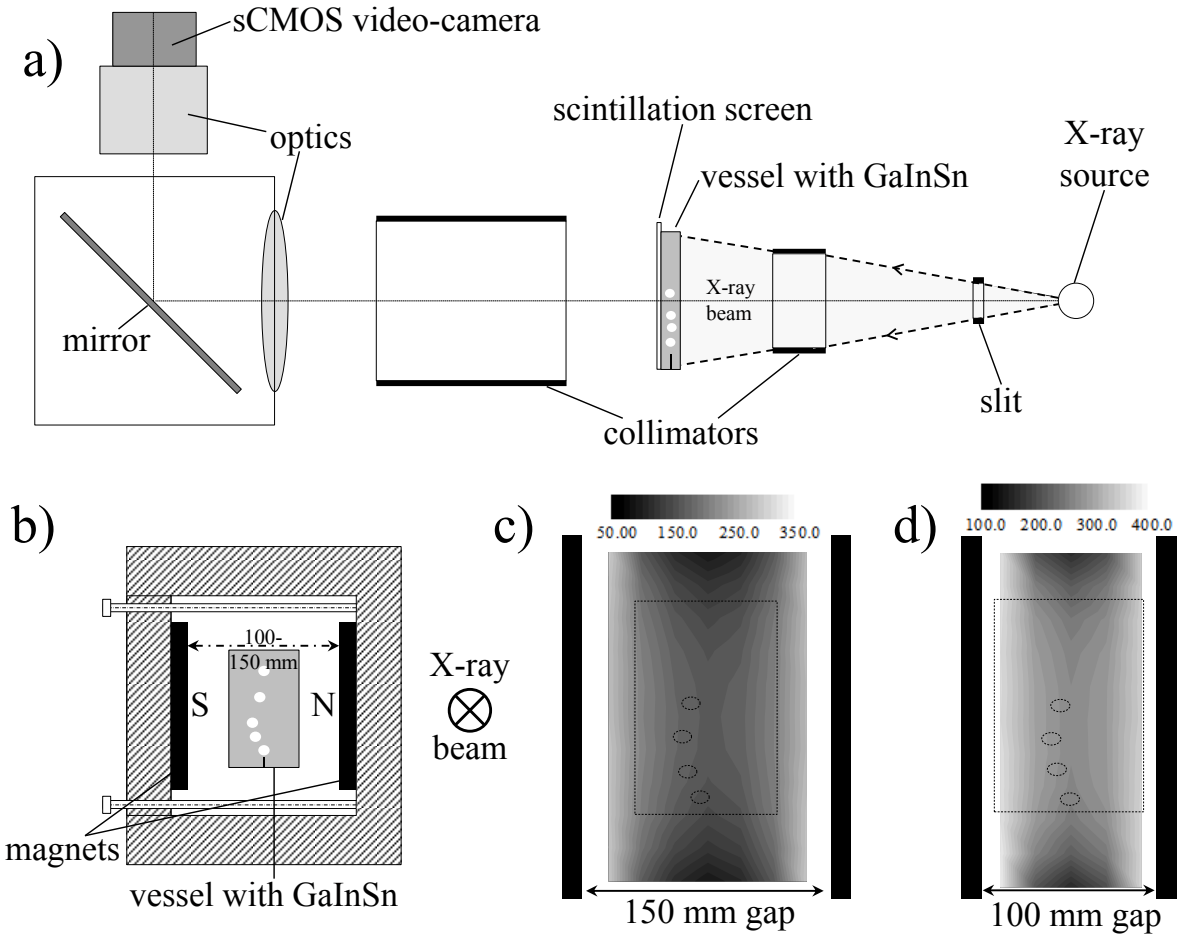

Figure 1. (a) Experimental setup (side view). (b) Magnet system (front view).(c-d) Distribution of the magnetic field strength for a pole shoe gap of 150 mm and 100 mm (in mT).

The high-speed video images were analyzed using Matlab scripts. Diverse parameters as bubble sizes, their trajectories, rising velocities and void fraction were extracted. The image processing was done as follows: as a first step a shading correction is performed by dividing the image by the mean reference image measured at zero gas flow rate. Separation of individual bubbles and bubble clusters from the background is achieved by using a threshold value which was slightly above 1 (i.e. ~1.07). All pixels whose brightness is above the threshold value were assigned to the bubble area. The corresponding threshold value is derived from a calibration measurement using 5 and 10 mm diameter glass balls surrounded by GaInSn at a zero gas flow rate and accounts X-ray scattering by the bubble surface. As a next step the images were analyzed applying the Matlab function *regionprops* which allows to extract parameters like perimeter, area, center of mass, etc. The bubble area is converted from pixel to metric values using the scaling of the image. Assuming a spherical bubble shape the mean bubble diameter was calculated according to

$$d_B = 2\sqrt{A_B/\pi}, \quad (2)$$

where A_B is the bubble projection area in the X-ray images. The rising velocity was calculated from the bubble trajectories according to

$$v = \frac{l}{\Delta t}, \quad (3)$$

where $l = \sqrt{(x_2 - x_1)^2 + (y_2 - y_1)^2}$ is the distance the bubble travelled between two subsequent bubble positions during the time step Δt = 1/150 s. The variables x and y denote the horizontal and vertical coordinates, respectively (see Figure 2). The time-averaged void fraction was calculated as

$$\alpha = \frac{1}{\mu T}\ln\left(\frac{I}{I_{ref}}\right), \quad (4)$$

where μ is the X-ray absorption coefficient, T = 12 mm is the thickness of the vessel in the direction of the X-ray beam, I is the actual time-averaged X-ray brightness the respective experiment and I_{ref} is the time-averaged X-ray brightness of the reference image measured at a zero gas flow rate. The absorption coefficient was estimated using the Beer-Lambert law

$$\mu = \frac{1}{T}\ln\left(\frac{I_0}{I}\right), \quad (5)$$

where I_0 is the time-averaged primary beam intensity after transition through the empty vessel. Additionally, it has to be considered that X-ray scattering due to the increasing interfacial area inside the vessel with increasing gas content leads to an increasing X-ray background signal and finally to an overestimation of the average gas void fraction. On the other hand, this effect is partly compensated by the resolution of the X-ray radiography since bubbles with diameters below 1 mm cannot be resolved leading to an underestimation of the gas void fraction.

It has to be mentioned at this point that an essential limitation of the experiment is the restriction of the dimension of fluid domain in the direction of the X-ray beam. This issue arises from the high X-ray attenuation coefficient of the liquid metal. The choice of a gap of 12 mm is a compromise, to be weighed between the best possible image contrast and the disturbed behavior of the bubbles due to the narrowness of the container. The distance of 12 mm between the side walls is in the same order of magnitude as the size of the bubbles at the highest gas flow rates. In general, constraining walls can cause an elongation of bubbles in the vertical direction, suppress secondary motion and alter the wake structure by reducing the wake volume and the rate of fluid circulation within the wake (Clift et al., 1978). Davenport et al. (1967) observed that the side wall effect reduces bubble rising velocity. Krishna et al. (1999) found that the rise velocity can be reduced in water by a factor of about 0.5 at maximum. Furthermore, the authors report that the bubble rise velocity becomes independent of the bubble diameter d_B for $d_B/D > 0.6$. Therefore, the influence of the side walls on bubble characteristics (trajectory, shape and velocity) is probably not negligible at high gas flow rates. In this work we focus on detailed investigations at moderate gas flow rates ≤ 400 cm^3/min where $d_B/D < 0.6$. This restriction allows minimizing the influence of the container walls on the bubble parameters.

Results and discussion

Figure 2 presents snapshots of bubble chains at different gas flow rates and magnetic fields recorded few seconds after the initiation of the gas injection. Typical videos of the gas injection for different gas flow rates can be viewed in the supplementary material where the left frame shows the bubble chain ascending without a magnetic field, and the middle and the right frames show bubble chains ascending in

the magnetic field for a pole shoe gap of 150 mm and 100 mm, respectively. In case without a magnetic field bubble size increases with increasing gas flow rate: the mean bubble diameter grows from 5.2±0.5 mm for 150 cm^3/min to 7.2±0.5 mm for 400 cm^3/min. Increasing bubble size leads to increasing buoyancy force and as a consequence the bubble velocity rises from 380±35 mm/s to 455±60 mm/s for 150 cm^3/min and 400 cm^3/min corresponding to Reynolds numbers of ~5985 and ~9922, respectively. The values for velocity are calculated for the bubble rising without a magnetic field, and are taken at a height of 60 mm above the nozzle and are ensemble-averaged over many bubbles. Moreover, the bubble shape changes from an almost elliptical shape for low gas flow rates to spherical cap shape at high gas flow rates which is a typical feature of increasing Reynolds number (Bhaga and Weber, 1981; Clift et al., 1978). Due to the bevel shape of the nozzle the bubble chain has a preferential path and the bubble chain is deflected to the right.

In contrast to single rising bubbles, bubbles rising in a chain are affected by the surrounding bubbles: bubble-wake interactions become an integral part of such a motion often manifesting itself in the formation of bubble pairs and groups (Badam et al., 2008; Kyriakides et al., 1997). It becomes obvious from the videos that the bubble pairing regime gets visible for the first time at 400 cm^3/min in the magnetic field compared to 300 cm^3/min for bubbles moving without a magnetic field (see also few bubble pairing examples highlighted in circles in Figure 2). The bubble pairing regime was found to be necessary for bubble coalescence (Keplinger et al., 2018), therefore its later occurrence in a magnetic field also shifts the onset of coalescence to higher gas flow rates $\geq$ 400 cm^3/min.

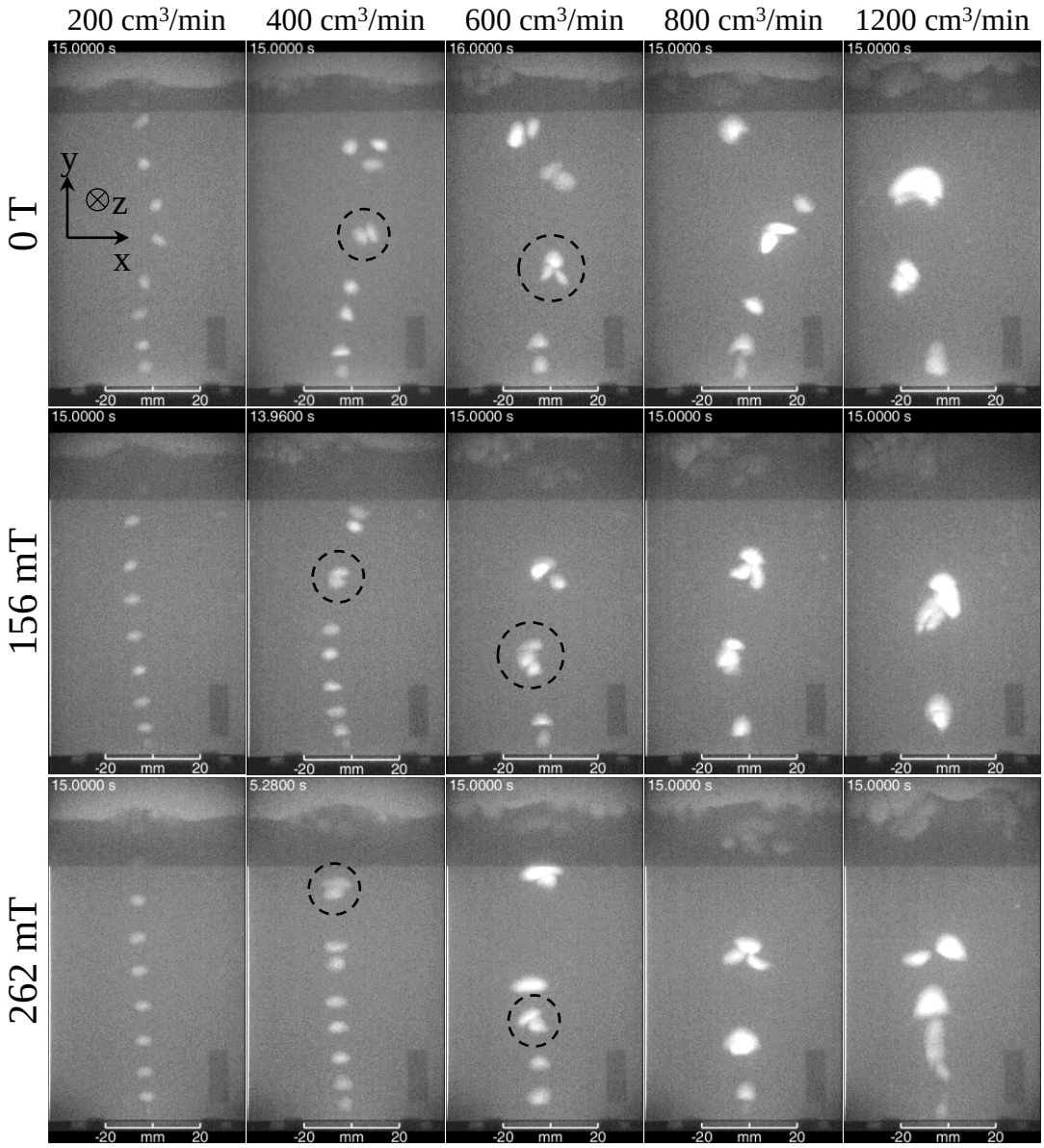

Figure 2. Snapshots of bubble chains at different gas flow rates and different magnetic fields.

Almost straight bubble chains with only minor perturbations produce an almost quasi-symmetrical flow with respect to the vertical centerline of the container. This flow pattern is often called “Gulfstream” or “double-cell turbulent flow” regime where the liquid is driven upwards by the bubbles in the middle of the column and flows downwards along the side walls forming two large vortices (Díaz et al., 2006; Freedman and Davidson, 1969). An increasing gas flow rate provokes a slight curvature of the bubble chain towards the side wall of the vessel (see videos of the supplementary material). Such an asymmetry can be explained by the transition from the double-cell turbulent flow regime to a steady flow regime with a dominating vortex on the right side of the vessel.

Figure 3 shows the time-averaged distributions of the void fraction which was calculated using eq. (4). In case of bubble chains rising without a magnetic field, no sharp contour of the bubble trajectory is formed. This can be attributed to the unsteady flow with frequent changes of the direction of bubble motion. The bubble chain shows pronounced oscillations leading to almost symmetrical distributions of

the time-averaged void fractions with a clear maximum along the centerline of the vessel (cf. Figure 3, first row). Such an oscillatory behavior of the bubble path was shown to be typical for liquid columns with narrow extensions and aspect ratios above 1.25 (Díaz et al., 2006). The characteristic frequency of path oscillations was well reproduced by numerical simulations (see for instance Liu et al. (2018)). Figure 3 reveals the turbulent dispersion of the gas bubbles which becomes more pronounced with increasing distance from the nozzle. In all experiments considered here the maximum value of the void fraction is found in a domain up to a height of 30 mm above the nozzle (i.e. in the region where the bubble accelerates from rest until reaching a steady terminal rising velocity). However, it becomes obvious that the magnetic field exerts a stabilizing effect on the bubble trajectories. The void fraction distributions are not so diffuse and the contour of the bubble chain becomes sharper and clearly recognizable. That means that fluctuations of the bubble motion are significantly reduced by the magnetic field, but, a distinct curvature of the bubble path survives at field strength of 156 mT. Similar observations with respect to the reduction of the dispersion coefficient by the magnetic field were reported for the case of a bubble plume in a vertical liquid sodium channel flow (Eckert et al., 2000a). As a result of numerical simulations Zhang et al. (2016) concluded that the horizontal motion of Argon bubbles rising in GaInSn is completely suppressed for a magnetic interaction parameter N of about unity (particularly, N > 0.93 for d_B =*4.3* mm and N > 1.07 for d_B = 6.4 mm). Mori et al. (1977) have reported that the motion of nitrogen bubbles of d_B ≤ 6 mm in mercury is restricted to the vertical direction when the magnetic field is about 1.5 T. In our experiments a considerable reduction of the curvature of the bubble trajectories is observed for the magnetic field strength of 262 mT (N ~ 0.5) (cf. Figure 3).

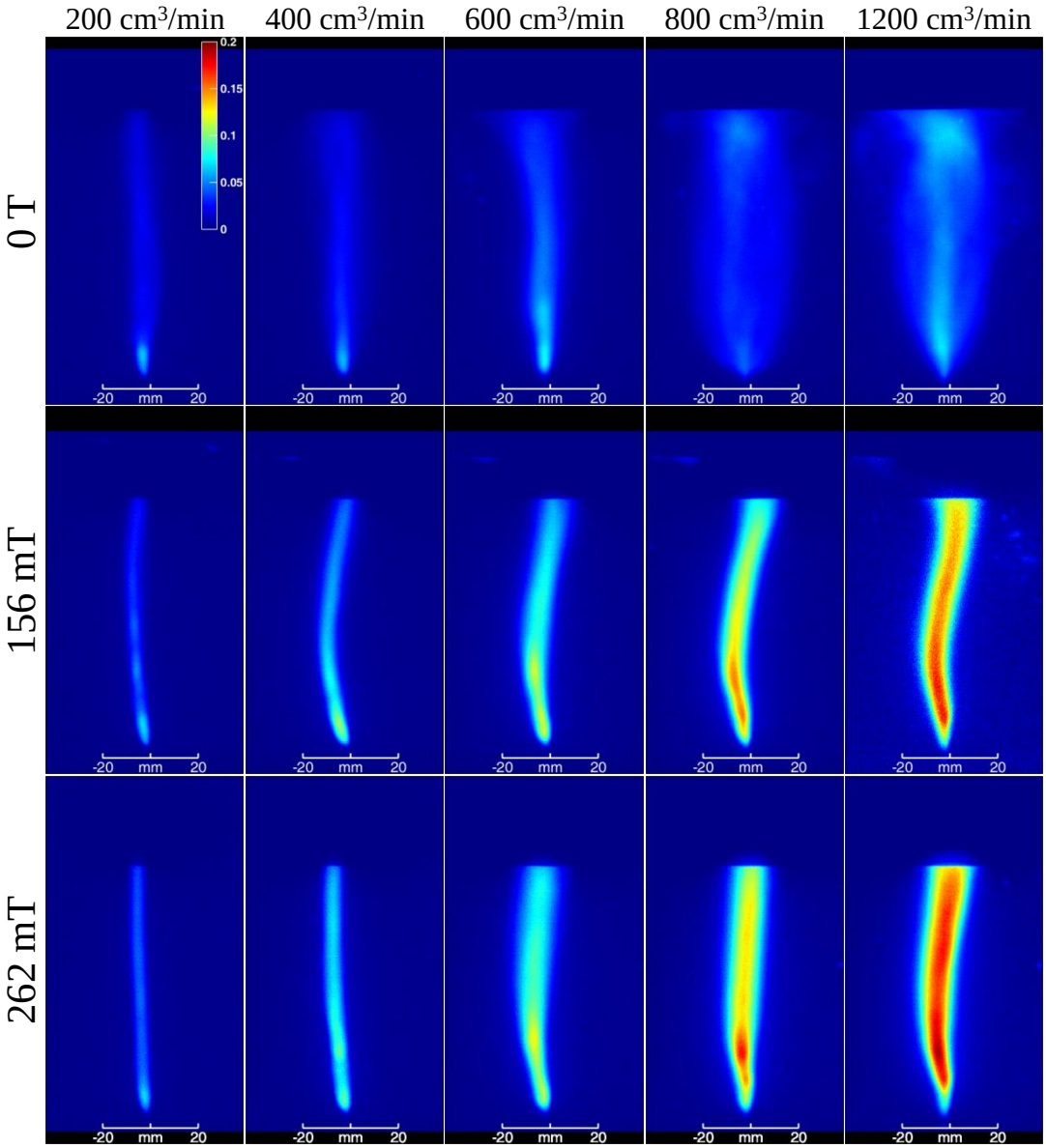

Figure 3. Time-averaged void fraction at different gas flow rates and different magnetic fields.

The evolution of selected essential bubble properties, namely bubble deformation, velocity and orientation, ensemble-averaged for the respective height are depicted in Figure 4. The bubble deformation was calculated as

$$A^* = \frac{S}{\pi d_B}, \qquad (6)$$

where S is the bubble perimeter. It is noticeable that the deformation parameter A^* features measurable oscillations (see fist row in Figure 4). When a magnetic field is applied, these oscillations are not significantly damped but even amplified especially at higher z-positions.

Similar oscillations can be observed for the bubble velocity. These oscillations are usually associated with the zig-zag motion of the rising bubbles (Di Marco et al., 2003; Schwarz and Fröhlich, 2014; Zhang et al., 2005). In the absence of a magnetic field these oscillations do not become visible in the time-averaged velocity. The explanation for this is evidently the same as in the case of the bubble trajectories:

the bubble motion without a magnetic field is rather random, any oscillatory behavior is blurred and disappears by averaging. This is a clear indication that the magnetic field produces a kind of synchronization of the bubble movement, i.e. deviations from a straight path associated with the zig-zag motion are not fully suppressed, but the trajectories of the individual bubbles movement become highly correlated. Moreover, the measurements show that the bubble rising velocities and their oscillation amplitudes decrease with increasing magnetic field. The bubble velocity (calculated from eq. (3)) decreases with increasing magnetic field strength to 352±22 mm/s at 156 mT (*Re*~5544, *N*~0.18, *Ha*~32) and to 320±11 mm/s at 262 mT (*Re*~5040, *N*~0.57, *Ha*~54) for 150 cm^3/min, to 438±39 mm/s at 156 mT (*Re*~9551, *N*~0.21, *Ha*~44) and to 358±24 mm/s at 262 mT (*Re*~7807, *N*~0.71, *Ha*~74) for 400 cm^3/min. This result is consistent with previous observations by Eckert et al. (2000b). Numerical calculations by Zhang et al. (2016) show that for the large bubbles (d_B = 6.4 mm) the mean bubble velocity monotonously decreases with increasing magnetic field for a magnetic interaction parameter larger than one. Jin et al. (2016) performed numerical simulations for large Argon bubble (d_B = 7 mm) rising in liquid steel. They predict a decrease of the bubble velocity by 25% for a transverse magnetic field of B = 0.5 T (N = 0.68). This is in a fairly good agreement with our experiments where a reduction of the velocity by approximately 22% was detected for bubbles having an equivalent diameter of 7.2 mm at B = 0.262 T (N ~ 0.71). The drop of the velocity is explained by the Lorentz force which breaks the motion of the liquid metal. As a result, the bubble needs more energy during its rise to displace the surrounding liquid metal causing a lower bubble velocity (Jin et al. (2016)). Zhang et al. (2016) have also reported that in the limit of large interaction parameters the bubble velocity reaches a critical minimal value which cannot be further reduced. This critical value corresponds approximately to one tens of the bubble rising velocity at the absence of magnetic field.

The highest amplitude of the velocity oscillations is observed at a gas flow rate of 300 cm^3/min. Here, the magnetic field causes a synchronization and regularization of the zig-zag motion while the zig-zag motion is almost suppressed by the magnetic field at lower gas flow rates. Further increase of the gas flow rate promotes bubble-wake interactions and as a result the harmonic zig-zag motion is disturbed and the amplitude of the velocity oscillations decreases. This moment can be identified as onset of the bubble pairing regime which corresponds to a gas flow rate of 400 cm^3/min.

The inclination angle of the major bubble axis with respect to the horizontal plane, here denoted as ‘orientation’, is obtained from fitting an ellipse to the bubble projection area. The corresponding plots shown in Figure 4 demonstrate that the bubbles tend to be oriented in the direction of the magnetic field and this effect becomes stronger the stronger the magnetic field. The curve for the case B = 0 is not shown here. The irregular fluctuations of the bubble path (cf. Figure 3) also cause a random orientation of the individual bubbles at the respective height positions. In consequence, the use of ensemble averaging yields near-zero orientation values for the entire fluid cell. Therefore, the diagrams dealing with the bubble orientation in Figure 4 do not contain any curve for the case without magnetic field. In this respect we also refer to the text below where we discuss the behavior of individual bubbles in the chain.

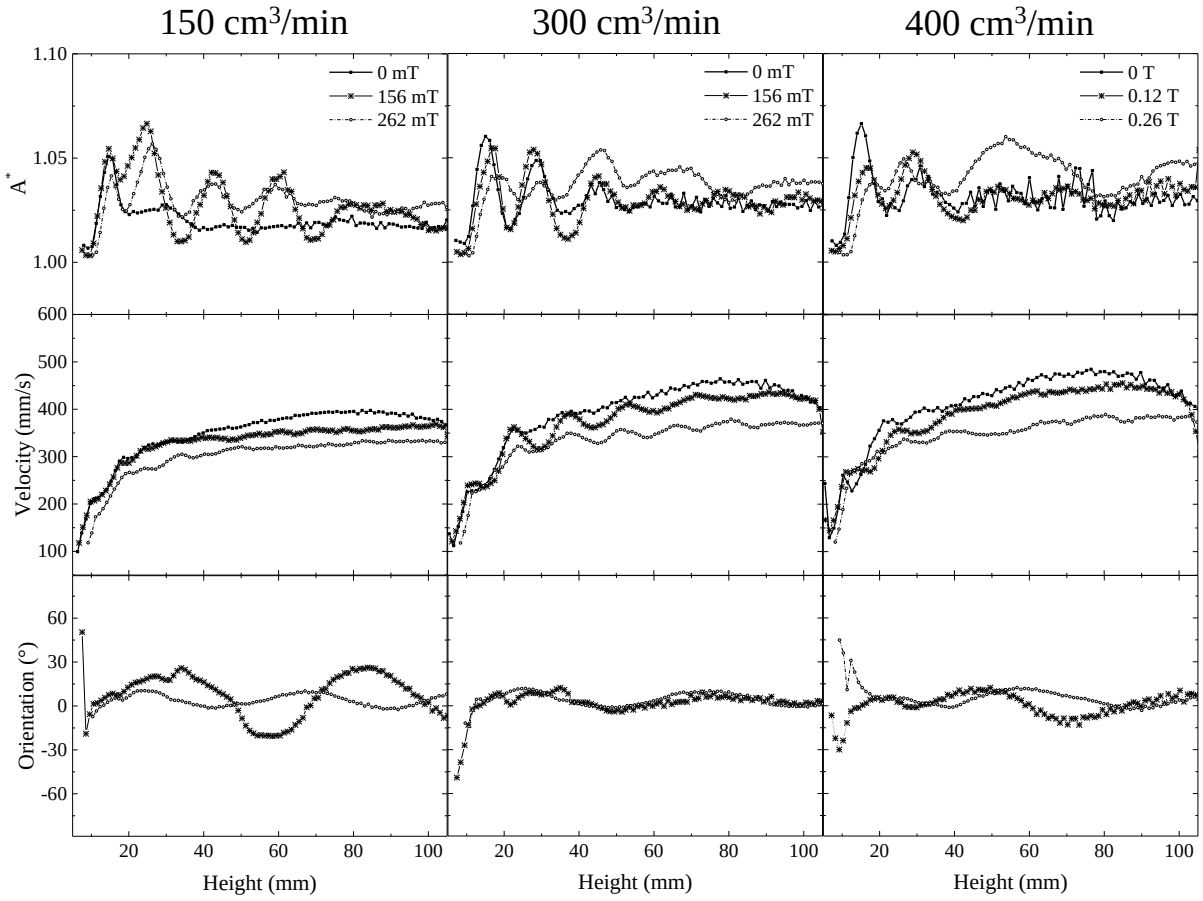

Figure 4. Bubble deformation (first row), bubble velocity (second row) and bubble orientation (third row) for 150 cm^3/min, 300 cm^3/min and 400 cm^3/min Ar gas flow rates (columns 1, 2 and 3 correspondingly).

Figure 5 shows the evolution of the bubble surface (first row) and major axis (second row) for an Ar gas flow rate of 200 cm^3/min. Figures 5 a-c illustrate three typical trajectories of individual bubbles without magnetic field (curved to the left, middle and right) representing different shapes of the bubble chain. Corresponding cases of bubbles moving under the influence of a magnetic field are shown in Figure 5 d and e for 156 mT and 262 mT, respectively. The Figures 5 a and b show the occurrence of the so-called initial path instability (PI) which is often characterized by extreme values of the orientation and a significant drop in the bubble horizontal velocity. Detailed description and explanation can be found in (Richter et al., 2018). Figure 4 demonstrates that upon application of a magnetic field, not only the bubble path becomes less curved, but also path instabilities are strongly suppressed. Since path instabilities are known to be a direct consequence of the wake instabilities (see for instance works by de Vries et al. (2002) and Zenit and Magnaudet (2008)) it additionally proves that the bubble wake is strongly affected by the magnetic field. Simulations carried out by Jin et al. (2016) for a magnetic field of 0.2 T show that the hairpin structures, that are generated by bubble shape oscillations, are reduced and elongated in the direction of the magnetic field. In addition, their twisting motion is suppressed (Zhang et al., 2016). Further increase of the magnetic field to 0.5 T significantly damps the complex wake structures behind the bubble and reduces the wake size (Jin et al., 2016). Numerical simulations by Jin et al. (2016) and Zhang et al. (2016) also show that the vorticity is aligned almost perfectly in the vertical direction.

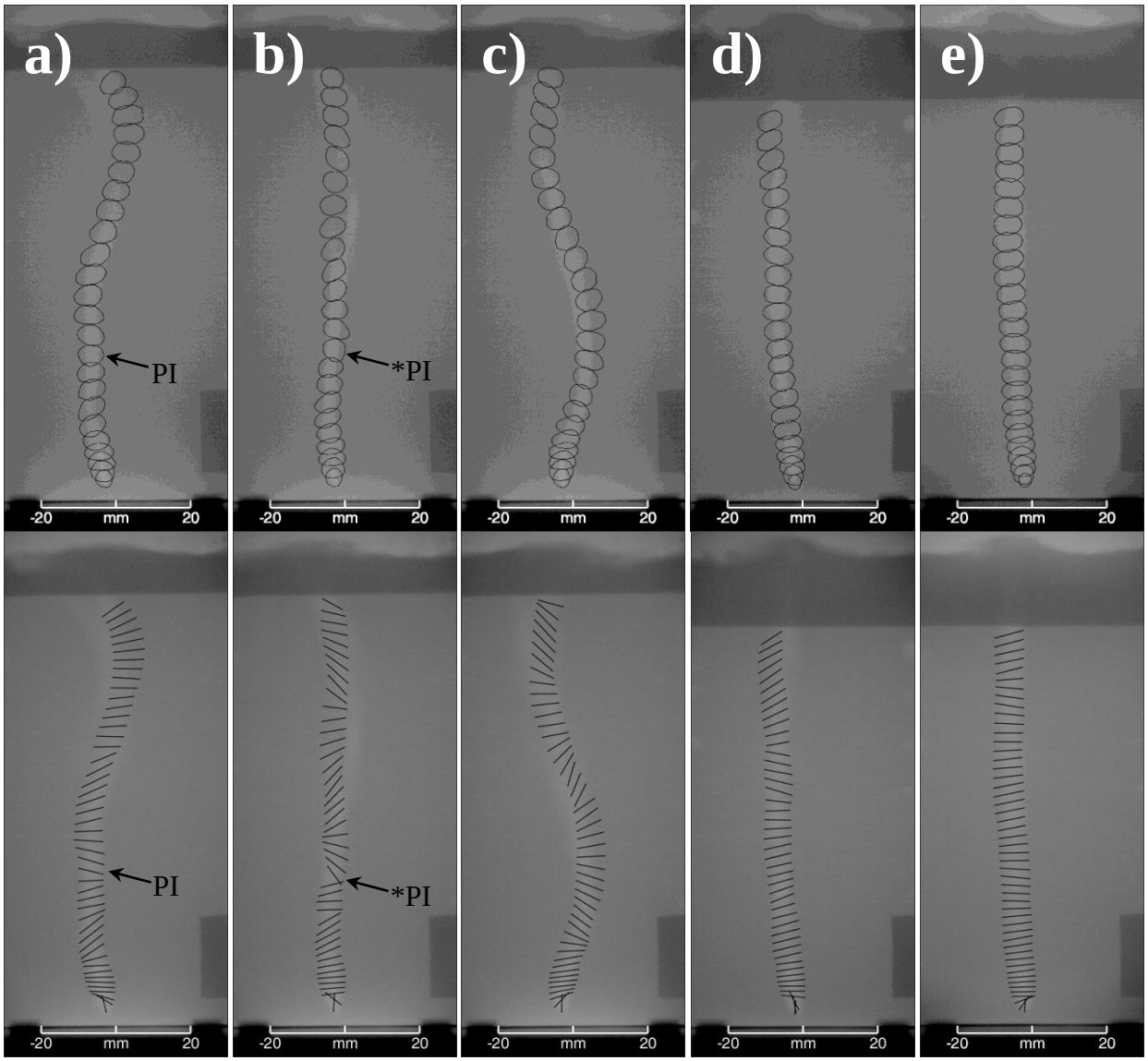

Figure 5. Evolution of the bubble surface (every second frame) and major axis at a gas flow rate of 200 cm^3/min: a-c) without magnetic field (PI indicates the occurrence of path instabilities), d) 156 mT, e) 262 mT. The background images represent X-ray brightness obtained through averaging over the bubble rising time.

Figure 6 provides quantitative results related to the particular bubbles shown in Figure 5. The strong scattering of the first data points in Figure 6 is due to the fact that in this area the bubbles have not yet completely detached from the nozzle. The bubble diameter oscillates periodically in the presence of magnetic field, while without magnetic field these oscillations are irregular (see the first row of Figure 6). Concerning the bubble shape presented in the second row, all bubbles reveal fluctuations, with the amplitude of the one in the strong magnetic field being the lowest. In addition, the shape is more flattened towards an ellipsoid. The third row of diagrams shows the bubble orientation. Additionally, a considerable reduction of the fluctuations in bubble orientation indicates an increasing alignment of the large bubble axis along the field lines with increasing field strength. Jin et al. (2016) predicted an elongation of the

bubble in the direction of the magnetic field as a result of the force distribution outside the bubble. The competition between Lorenz force and pressure gradient results in the formation of two vortices along the magnetic field direction on both ends of the bubble. On the other hand, no similar vortices are formed in the direction perpendicular to the magnetic field, and as a consequence the bubble is squeezed and elongated in the direction of the magnetic field (Jin et al., 2016; Zhang et al., 2016). Zhang et al. (2016) also reported that these vortices disappear for $N \gg 1$ and the bubbles tend to return to a spherical shape.

In accordance with Figure 4, it becomes also evident here that the mean bubble velocity and its fluctuations are reduced in the magnetic field (see the fourth row). Without a magnetic field the velocity of individual bubbles shows irregular oscillations. In turn, Richter et al. (2018) have demonstrated that in case when individual bubbles move through a stagnant liquid the velocity oscillations are periodic. Therefore, this irregularity indicates that the zig-zag motion of the bubbles is disturbed by the bubble wakes of preceding bubbles and by the turbulent flow developed in the vessel.

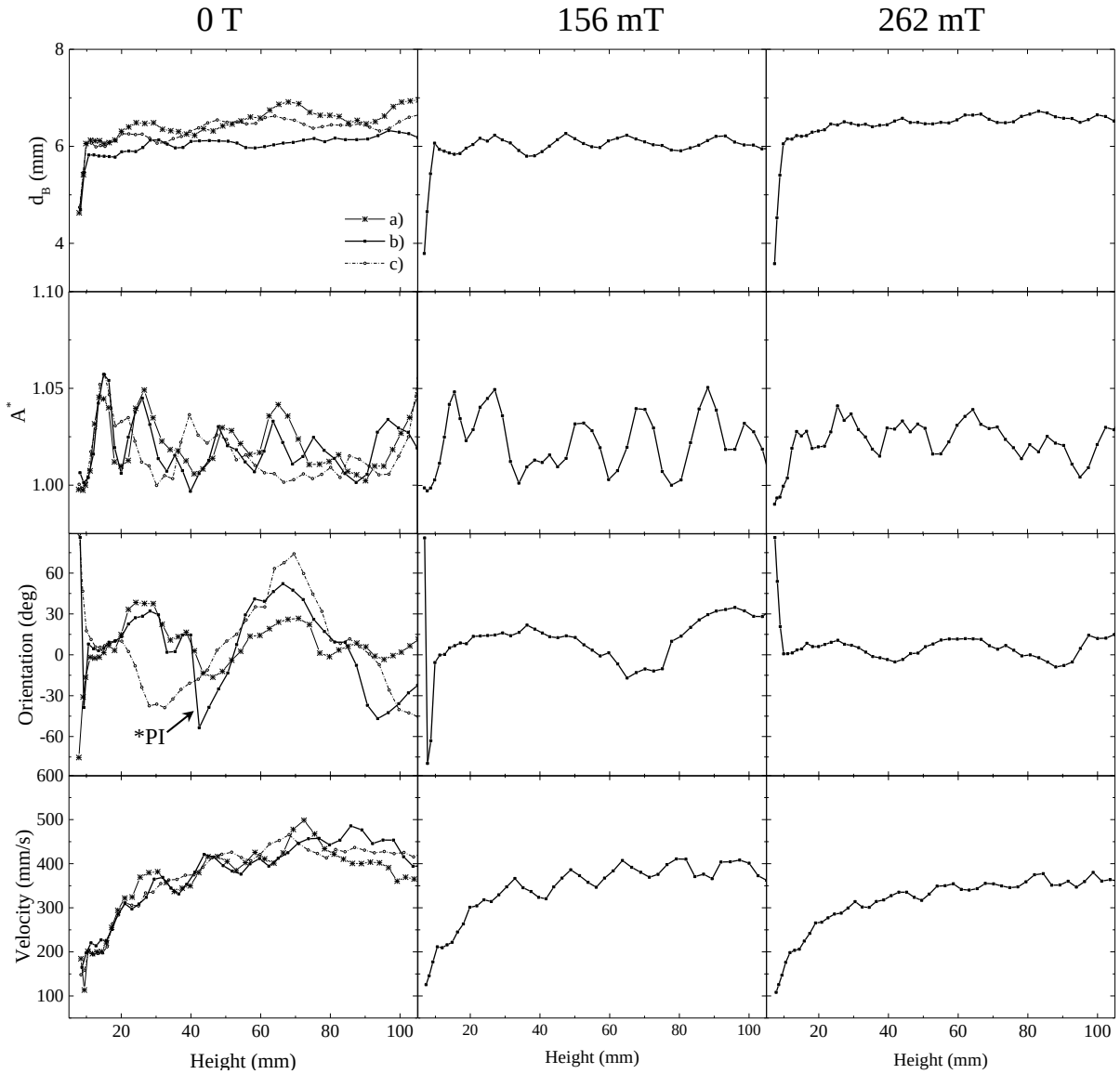

Figure 6. Mean bubble diameter (first row), bubble deformation (second row), bubble velocity (third row) and bubble orientation (fourth row) at a gas flow rate of 200 cm^3/min for the bubble cases shown in Figure 5 a-c (left column), d (middle column) and e (right column).

Summary and conclusions

This work presents an experimental investigation of bubble chains rising in a liquid metal under the influence of a horizontal magnetic field. The dynamics of the bubbly flow was visualized using X-ray radiography.

The lateral dispersion of the rising gas bubbles is governed by the turbulent flow in the liquid metal which triggers pronounced oscillations of the bubble trajectories and thus of the bubble chain which does not show a sharp contour. As a consequence, the time-averaged gas distribution appears to be symmetric with respect to the nozzle position in the case without magnetic field. The application of the magnetic field suppresses turbulent fluctuations and causes an alignment of the vorticity in the bubble wake. A striking feature of the bubbly flow structure in the magnetic field is the emergence of the bubble chain contour in the time-averaged images. So, a main effect of the magnetic field is to synchronize the movement of the individual bubbles. This leads to a regularization of the bubble zig-zag motion at moderate magnetic fields or at higher fields and higher gas flow rates, while the zig-zag motion is almost suppressed by the magnetic field at lower gas flow rates.

This effect becomes also evident in the time-averaged curves of main bubble parameters (orientation, deformation, velocity) that reveal regular oscillations if a magnetic field is applied. Bubble chains rising in a magnetic field do not oscillate in time, but decline towards one side wall of the vessel leading to an asymmetric gas distribution. The application of a sufficiently strong magnetic field suppresses the zig-zag motion of the bubbles and forces them to follow a straight path.

The oscillation amplitudes of both the bubble deformation and orientation are damped by the strongest magnetic field used in our experiments (B ~ 262 mT). The ellipsoidal bubbles tend to align their major axes along the magnetic field. Measurements of the reduction of the bubble velocity by the magnetic field are in a good agreement with predictions from numerical simulations in the literature (Jin et al., 2016).

The case of higher gas flow rates was not systematically investigated in this study with respect to the quantitative determination of the bubble properties. In the parameter range of Q_{gas} > 400 cm^3/min, bubble pairing occurs and the bubbles start to form clusters. Frequently occurring interactions among the bubbles (collisions, coalescence and breakup) coupled with strong bubble shape deformations make it very difficult to obtain accurate values of the equivalent bubble diameter, velocity and deformation. The flow regime becomes more complex and the turbulence level increases significantly. The bubble shape changes to spherical cap and the magnetic field strengths considered here do not show an obvious impact on such highly turbulent flow regimes.

Acknowledgments

The authors are grateful to the German Helmholtz Association for the financial support in form of the Helmholtz-Alliance “LIMTECH”.

Literature

Baake, E., Fehling, T., Musaeva, D., Steinberg, T., 2017. Neutron radiography for visualization of liquid metal processes: bubbly flow for CO_2 free production of Hydrogen and solidification processes in EM field. IOP Conf. Ser. Mater. Sci. Eng. 228, 012026. https://doi.org/10.1088/1757-

899X/228/1/012026
Badam, V.K., Buwa, V., Durst, F., 2008. Experimental investigations of regimes of bubble formation on submerged orifices under constant flow condition. Can. J. Chem. Eng. 85, 257–267. https://doi.org/10.1002/cjce.5450850301
Bhaga, D., Weber, M.E., 1981. Bubbles in viscous liquids: shapes, wakes and velocities. J. Fluid Mech. 105, 61–85. https://doi.org/10.1017/S002211208100311X
Clift, R., Grace, J.R., Weber, M.E., 1978. Bubbles, Drops, and Particles. Acad. Press.
Davenport, W.G., Bradshaw, A.V., Richardson, F.D., 1967. Behaviour of spheriacl cap bubbles in liquid metals. J. Iron Steel Steel Inst. 1034–1042.
Davis, K.G., Irons, G.A., Guthrie, R.I.L., 1978. X-Ray Cinematographic Observations of Gas Injection into Liquid Metals. Metall. Trans. B 9, 721–722. https://doi.org/10.1007/BF03257224
de Vries, A.W.G., Biesheuvel, A., van Wijngaarden, L., 2002. Notes on the path and wake of a gas bubble rising in pure water. Int. J. Multiph. Flow 28, 1823–1835. https://doi.org/10.1016/S0301-9322(02)00036-8
Di Marco, P., Grassi, W., Memoli, G., 2003. Experimental study on rising velocity of nitrogen bubbles in FC-72. Int. J. Therm. Sci. 42, 435–446. https://doi.org/10.1016/S1290-0729(02)00044-3
Díaz, M.E., Montes, F.J., Galán, M.A., 2006. Influence of Aspect Ratio and Superficial Gas Velocity on the Evolution of Unsteady Flow Structures and Flow Transitions in a Rectangular Two-Dimensional Bubble Column. https://doi.org/10.1021/IE060466B
Eckert, S., Gerbeth, G., Lielausis, O., 2000a. The behaviour of gas bubbles in a turbulent liquid metal magnetohydrodynamic flow: Part I: Dispersion in quasi-two-dimensional magnetohydrodynamic turbulence. Int. J. Multiph. Flow 26, 45–66. https://doi.org/10.1016/S0301-9322(99)00006-3
Eckert, S., Gerbeth, G., Lielausis, O., 2000b. The behaviour of gas bubbles in a turbulent liquid metal magnetohydrodynamic flow: Part II: Magnetic field influence on the slip ratio. Int. J. Multiph. Flow 26, 67–82. https://doi.org/10.1016/S0301-9322(99)00007-5
Freedman, W., Davidson, J., 1969. Hold-up and liquid circulation in bubble columns. Trans. Inst. Chem. Eng. 47, 251–262.
Fröhlich, J., Schwarz, S., Heitkam, S., Santarelli, C., Zhang, C., Vogt, T., Boden, S., Andruszkiewicz, A., Eckert, K., Odenbach, S., Eckert, S., 2013. Influence of magnetic fields on the behavior of bubbles in liquid metals. Eur. Phys. J. Spec. Top. 220, 167–183. https://doi.org/10.1140/epjst/e2013-01805-4
Gundrum, T., Büttner, P., Dekdouk, B., Peyton, A., Wondrak, T., Galindo, V., Eckert, S., 2016. Contactless Inductive Bubble Detection in a Liquid Metal Flow. Sensors 16, 63. https://doi.org/10.3390/s16010063
Heindel, T.J., 2011. A Review of X-Ray Flow Visualization With Applications to Multiphase Flows. J. Fluids Eng. 133, 074001. https://doi.org/10.1115/1.4004367
Iguchi, M., Chihara, T., Takanashi, N., Ogawa, Y., Tokumitsu, N., Morita, Z., 1995. X-ray Fluoroscopic Observation of Bubble Characteristics in a Molten Iron Bath. ISIJ Int. 35, 1354–1361. https://doi.org/10.2355/isijinternational.35.1354
Iguchi, M., Nakatani, T., Kawabata, H., 1997. Development of a multineedle electroresistivity probe for measuring bubble characteristics in molten metal baths. Metall. Mater. Trans. B 28, 409–416. https://doi.org/10.1007/s11663-997-0106-3
Jin, K., Kumar, P., Vanka, S.P., Thomas, B.G., 2016. Rise of an argon bubble in liquid steel in the presence of a transverse magnetic field. Phys. Fluids 28, 093301. https://doi.org/10.1063/1.4961561
Kastengren, A., Powell, C.F., 2014. Synchrotron X-ray techniques for fluid dynamics. Exp. Fluids 55, 1686. https://doi.org/10.1007/s00348-014-1686-8
Keplinger, O., Shevchenko, N., Eckert, S., 2018. Visualization of bubble coalescence in bubble chains rising in a liquid metal. Int. J. Multiph. Flow 105, 159–169. https://doi.org/10.1016/J.IJMULTIPHASEFLOW.2018.04.001
Keplinger, O., Shevchenko, N., Eckert, S., 2017. Validation of X-ray radiography for characterization of gas bubbles in liquid metals. IOP Conf. Ser. Mater. Sci. Eng. 228, 012009. https://doi.org/10.1088/1757-899X/228/1/012009
Krishna, R., Urseanu, M.I., van Baten, J.M., Ellenberger, J., 1999. Wall effects on the rise of single gas

bubbles in liquids. Int. Commun. Heat Mass Transf. 26, 781–790. https://doi.org/10.1016/S0735-1933(99)00066-4
Kyriakides, N.K., Kastrinakis, E.G., Nychas, S.G., Goulas, A., 1997. Bubbling from nozzles submerged in water: Transitions between bubbling regimes. Can. J. Chem. Eng. 75, 684–691. https://doi.org/10.1002/cjce.5450750405
Liu, L., Keplinger, O., Ma, T., Ziegenhein, T., Shevchenko, N., Eckert, S., Yan, H., Lucas, D., 2018. Euler-Euler simulation and X-ray measurement of bubble chain in a shallow container filled with liquid metals. Chem. Eng. Sci. 192. https://doi.org/10.1016/j.ces.2018.07.034
Liu, L., Keplinger, O., Ziegenhein, T., Shevchenko, N., Eckert, S., Yan, H., Lucas, D., 2019. Euler–Euler modeling and X-ray measurement of oscillating bubble chain in liquid metals. Int. J. Multiph. Flow 110, 218–237. https://doi.org/10.1016/j.ijmultiphaseflow.2018.09.011
Lyu, Z., Karcher, C., 2016. Experimental study on bubble rising in liquid GaInSn using Local Lorentz Force Velocimetry (LLFV). Proc. 10th PAMIR Int. Conf. Fundam. Appl. MHD (Cagliary, Italy) 243–246.
Manera, A., Ozar, B., Paranjape, S., Ishii, M., Prasser, H.-M., 2009. Comparison between wire-mesh sensors and conductive needle-probes for measurements of two-phase flow parameters. Nucl. Eng. Des. 239, 1718–1724. https://doi.org/10.1016/j.nucengdes.2008.06.015
Mishima, K., Hibiki, T., Saito, Y., Nishihara, H., Tobita, Y., Konishi, K., Matsubayashi, M., 1999. Visualization and measurement of gas-liquid metal two-phase flow with large density difference using thermal neutrons as microscopic probes. Nucl. Instruments Methods Phys. Res. Sect. A Accel. Spectrometers, Detect. Assoc. Equip. 424, 229–234. https://doi.org/10.1016/S0168-9002(98)01300-X
Mori, Y., Hijikata, K., Kuriyama, I., 1977. Experimental Study of Bubble Motion in Mercury With and Without a Magnetic Field. J. Heat Transfer 99, 404. https://doi.org/10.1115/1.3450710
Mudde, R.F., 2010. Advanced measurement techniques for GLS reactors. Can. J. Chem. Eng. 88, n/a-n/a. https://doi.org/10.1002/cjce.20315
Mudde, R.F., Alles, J., van der Hagen, T.H.J.J., 2008. Feasibility study of a time-resolving x-ray tomographic system. Meas. Sci. Technol. 19, 085501. https://doi.org/10.1088/0957-0233/19/8/085501
Oryall, G.N., Brimacombe, J.K., 1976. The physical behavior of a gas jet injected horizontally into liquid metal. Metall. Trans. B 7, 391–403. https://doi.org/10.1007/BF02652710
Plevachuk, Y., Sklyarchuk, V., Eckert, S., Gerbeth, G., Novakovic, R., 2014. Thermophysical Properties of the Liquid Ga–In–Sn Eutectic Alloy. J. Chem. Eng. Data 59, 757–763. https://doi.org/10.1021/je400882q
Richter, T., Keplinger, O., Shevchenko, N., Wondrak, T., Eckert, K., Eckert, S., Odenbach, S., 2018. Single bubble rise in GaInSn in a horizontal magnetic field. Int. J. Multiph. Flow 104, 32–41. https://doi.org/10.1016/J.IJMULTIPHASEFLOW.2018.03.012
Saito, Y., Mishima, K., Tobita, Y., Suzuki, T., Matsubayashi, M., Lim, I.C., Cha, J.E., 2005. Application of high frame-rate neutron radiography to liquid-metal two-phase flow research. Nucl. Instruments Methods Phys. Res. A 542, 168–174. https://doi.org/10.1016/j.nima.2005.01.095
Sarma, M., Ščepanskis, M., Jakovičs, A., Thomsen, K., Nikoluškins, R., Vontobel, P., Beinerts, T., Bojarevičs, A., Platacis, E., 2015. Neutron Radiography Visualization of Solid Particles in Stirring Liquid Metal. Phys. Procedia 69, 457–463. https://doi.org/10.1016/J.PHPRO.2015.07.064
Schwarz, S., Fröhlich, J., 2014. Numerical study of single bubble motion in liquid metal exposed to a longitudinal magnetic field. Int. J. Multiph. Flow 62, 134–151. https://doi.org/10.1016/j.ijmultiphaseflow.2014.02.012
Shevchenko, N., Boden, S., Eckert, S., Borin, D., Heinze, M., Odenbach, S., 2013. Application of X-ray radioscopic methods for characterization of two-phase phenomena and solidification processes in metallic melts. Eur. Phys. J. Spec. Top. 220, 63–77. https://doi.org/10.1140/epjst/e2013-01797-y
Timmel, K., Eckert, S., Gerbeth, G., Stefani, F., Wondrak, T., 2010. Experimental Modeling of the Continuous Casting Process of Steel Using Low Melting Point Metal Alloys - the LIMMCAST Program. ISIJ Int. 50, 1134–1141. https://doi.org/10.2355/isijinternational.50.1134

Timmel, K., Shevchenko, N., Röder, M., Anderhuber, M., Gardin, P., Eckert, S., Gerbeth, G., 2015. Visualization of Liquid Metal Two-phase Flows in a Physical Model of the Continuous Casting Process of Steel. Metall. Mater. Trans. B 46, 700–710. https://doi.org/10.1007/s11663-014-0231-8

Vogt, T., Boden, S., Andruszkiewicz, A., Eckert, K., Eckert, S., Gerbeth, G., 2015. Detection of gas entrainment into liquid metals. Nucl. Eng. Des. 294, 16–23. https://doi.org/10.1016/j.nucengdes.2015.07.072

Wang, Z., Mukai, K., Izu, D., 1999. Influence of Wettability on the Behavior of Argon Bubbles and Fluid Flow inside the Nozzle and Mold. ISIJ Int. 39, 154–163. https://doi.org/10.2355/isijinternational.39.154

Wang, Z.H., Wang, S.D., Meng, X., Ni, M.J., 2017. UDV measurements of single bubble rising in a liquid metal Galinstan with a transverse magnetic field. Int. J. Multiph. Flow 94, 201–208. https://doi.org/10.1016/j.ijmultiphaseflow.2017.05.001

Xie, Y., Oeters, F., 1994. Measurements of bubble plume behaviour and flow velocity in gas stirred liquid Wood's metal with an eccentric nozzle position. Steel Res. 65, 315–319. https://doi.org/10.1002/srin.199401077

Xie, Y., Orsten, S., Oeters, F., 1992. Behaviour of Bubbles at Gas Blowing into Liquid Wood's Metal. ISIJ Int. 32, 66–75. https://doi.org/10.2355/isijinternational.32.66

Zenit, R., Magnaudet, J., 2008. Path instability of rising spheroidal air bubbles: A shape-controlled process. Phys. Fluids 20, 061702. https://doi.org/10.1063/1.2940368

Zhang, C., Eckert, S., Gerbeth, G., 2007a. Modification of Bubble-driven Liquid Metal Flows under the Influence of a DC Magnetic Field. ISIJ Int. 47, 795–801. https://doi.org/10.2355/isijinternational.47.795

Zhang, C., Eckert, S., Gerbeth, G., 2007b. The flow structure of a bubble-driven liquid-metal jet in a horizontal magnetic field. J. Fluid Mech. 575, 57. https://doi.org/10.1017/S0022112006004423

Zhang, C., Eckert, S., Gerbeth, G., 2005. Experimental study of single bubble motion in a liquid metal column exposed to a DC magnetic field. Int. J. Multiph. Flow 31, 824–842. https://doi.org/10.1016/j.ijmultiphaseflow.2005.05.001

Zhang, J., Ni, M.-J., 2014. Direct simulation of single bubble motion under vertical magnetic field: Paths and wakes. Phys. Fluids 26, 102102. https://doi.org/10.1063/1.4896775

Zhang, J., Ni, M.-J., Moreau, R., 2016. Rising motion of a single bubble through a liquid metal in the presence of a horizontal magnetic field. Phys. Fluids 28, 032101. https://doi.org/10.1063/1.4942014